Published March 28, 2011

System analysis shows distinct mechanisms and common principles of nuclear envelope protein dynamics

Nikolaj Zuleger,[1] David A. Kelly,[1] A. Christine Richardson,[4] Alastair R. W. Kerr,[1] Martin W. Goldberg,[4] Andrew B. Goryachev,[2,3] and Eric C. Schirmer[1,2]

[1]The Wellcome Trust Centre for Cell Biology, [2]Institute of Cell Biology, and [3]Centre for Systems Biology, The University of Edinburgh, Edinburgh EH9 3JR, Scotland, UK
[4]School of Biological and Biomedical Sciences, Durham University, Durham DH1 3LE, England, UK

The nuclear envelope contains >100 transmembrane proteins that continuously exchange with the endoplasmic reticulum and move within the nuclear membranes. To better understand the organization and dynamics of this system, we compared the trafficking of 15 integral nuclear envelope proteins using FRAP. A surprising 30-fold range of mobilities was observed. The dynamic behavior of several of these proteins was also analyzed after depletion of ATP and/or Ran, two functions implicated in endoplasmic reticulum–inner nuclear membrane translocation. This revealed that ATP- and Ran-dependent translocation mechanisms are distinct and not used by all inner nuclear membrane proteins. The Ran-dependent mechanism requires the phenylalanine-glycine (FG)-nucleoporin Nup35, which is consistent with use of the nuclear pore complex peripheral channels. Intriguingly, the addition of FGs to membrane proteins reduces FRAP recovery times, and this also depends on Nup35. Modeling of three proteins that were unaffected by either ATP or Ran depletion indicates that the wide range in mobilities could be explained by differences in binding affinities in the inner nuclear membrane.

Introduction

The nuclear envelope (NE) is a complex double membrane system. The outer nuclear membrane (ONM) is continuous with the ER (Callan et al., 1949) and seamlessly flows into the inner nuclear membrane (INM) where nuclear pore complexes (NPCs) are inserted (Prunuske and Ullman, 2006). At these sites, the NE bends into a unique structure with both convex and concave curvature called the pore membrane. Many NE transmembrane proteins (NETs), after their synthesis in the ER, spend most of their lifetime bound within the INM to the polymer of intermediate filament lamins (Gruenbaum et al., 2005; Schirmer and Foisner, 2007). Thus, NETs must dynamically exchange between several distinct populations located in the ER, the ONM, and free and tethered fractions in the INM.

The exchange step between ONM and INM is not fully understood, although it is generally accepted that it occurs where NPCs are inserted in the membrane. NPCs are symmetrical >40-MDa structures built from >30 distinct proteins called nucleoporins or Nups (Suntharalingam and Wente, 2003). Transport of soluble molecules through the NPC central channel is well documented, requiring transport receptors (importins/karyopherins) that interact with Nups carrying phenylalanine-glycine (FG) repeats (Suntharalingam and Wente, 2003). Transport of integral proteins is less certain; however, between the NPC and the membrane are less-characterized ∼100-Å peripheral channels (Reichelt et al., 1990; Hinshaw et al., 1992) that could allow transmembrane proteins to transit bidirectionally between the ONM and the INM by lateral diffusion.

Early studies supported use of the peripheral channels because increasing the nucleoplasmic mass of INM proteins above the 60-kD threshold predicted by the size of the channels blocked their INM accumulation (Soullam and Worman, 1995). These studies proposed that INM proteins freely exchanged between the ER and INM, but were retained in the INM by lamin

Correspondence to Eric Schirmer: e.schirmer@ed.ac.uk

Abbreviations used in this paper: INM, inner nuclear membrane; LAP, lamina-associated polypeptide; LBR, lamin B receptor; NE, nuclear envelope; NET, NE transmembrane protein; NPC, nuclear pore complex; ONM, outer nuclear membrane; PA, photoactivation; WT, wild type.

Supplemental Material can be found at:
http://jcb.rupress.org/content/suppl/2011/03/25/jcb.201009068.DC1.html
Original image data can be found at:
http://jcb-dataviewer.rupress.org/jcb/browse/3270

The Rockefeller University Press $30.00
J. Cell Biol. Vol. 193 No. 1 109–123
www.jcb.org/cgi/doi/10.1083/jcb.201009068

Published March 28, 2011

Table I. **Properties of NETs in this study**

NET	$t_{1/2}$	NLS score[a]	Nucleoplasmic aa (+GFP)[b]	Total residues	Nucleoplasmic isoelectric point	Transmembrane helices
NET51	7.1	−0.22	18 (266)[c]	140	11.65	4
NET39	13.7	−0.47	76[p] (334)[d]	201	10.84	3
NET30	14.2	−0.47	177 (439)[c] (38)[d]	235	9.16	2
NET55	14.9	−0.47	53 (301)[d]	257	8.8	6
NET20	18.0	−0.47	39[p] (499)[d]	356	10.23	1
NET37	19.3	−0.47	22[d]	680	10.47	1
Emerin	20.3	0.02	223[d]	254	5.37	1
LBR	20.9	1.19	343 (589)[d]	615	10.19	8
NET59	21.0	−0.47	25 (278)[d]	552	7.54	2
NET47	23.3	−0.47	185[d]	418	8.8	7
LAP2[e]	25.0	0.21	410[d]	454	9.94	1
SUN2	32.6	−0.16	212 (460)[d]	717	10.07	1
NET33	48.3	0.06	59[c]	495	7.29	1
LAP1-S[e]	105.7	0.02	310[df]	506	8.25	1
LAP1-L[e]	233.5	0.02	337[df]	583	6.73	1

[a]NLS prediction scores were generated by PSORTII (Nakai and Horton, 1999).

[b]Nucleoplasmic aa was calculated for untagged proteins using transmembrane predictions from TMHMM v2.0. If the GFP fusion was predicted to be nucleoplasmic, then the total predicted aa with linker sizes plus GFP residues is included in parentheses.

[c]Calculations were determined entirely by TMHMM prediction.

[d]Calculations were modified based on direct testing of membrane/C-terminus topology through GFP antibody accessibility in digitonin permeabilized cells.

[e]Rat protein.

[f]Transmembrane spans for these proteins failed to reach the threshold of the TMHMM algorithm, so numbers were calculated based on the position of the ∼80% calculated spans for LAP1.

binding (Powell and Burke, 1990; Soullam and Worman, 1993). Recent studies have suggested that this exchange/translocation is more complex than free diffusion, with one finding an energy requirement (Ohba et al., 2004), others showing involvement of components used for NPC transport of soluble proteins (King et al., 2006; Theerthagiri et al., 2010; Turgay et al., 2010), and yet another supporting a signal sequence–mediated event initiated in the ER (Saksena et al., 2004, 2006; Braunagel et al., 2007).

To better understand NE dynamics, we directly compared several INM proteins using a combination of FRAP and photoactivation (PA) experiments in both the ER and the NE. These data indicated that for many NETs, binding in the INM is so stable that recovery after photobleaching depended more on exchange of proteins between the ER and INM than on mobility within the INM. Indeed, modeling of the data for three NETs that appear to translocate by free diffusion was consistent with the significant exchange between the ER and INM, whereas the differences in the observed FRAP half-lives of these proteins were shown to be largely dependent on their binding affinities in the INM. Testing the effects of blocking various proposed translocation mechanisms on the FRAP mobilities of several INM proteins suggests the existence of at least four distinct mechanisms: (1) one requiring ATP but not Ran, (2) one requiring Ran GTPase function but not ATP, (3) one requiring neither Ran nor ATP, and (iv) one that is facilitated by addition of FGs but that is not Ran dependent. Finally, two of these mechanisms depended on the NPC protein Nup35 (Nup53p in yeast) that faces the peripheral channels in yeast (Alber et al., 2007), which is consistent with previous studies arguing for translocation through these channels (Soullam and Worman, 1993, 1995; Ohba et al., 2004).

Results

Comparison of 15 INM proteins by FRAP reveals a 30-fold range in recovery half-times

Previous FRAP studies on INM proteins used varied photobleaching parameters and cell types and thus could not be used to directly compare motility of these different proteins in the NE (Ellenberg et al., 1997; Ostlund et al., 1999; Wu et al., 2002; Shimi et al., 2004). To obtain a more systematic perspective, a collection of 15 confirmed INM NETs (Senior and Gerace, 1988; Worman et al., 1988; Foisner and Gerace, 1993; Smith and Blobel, 1994; Squarzoni et al., 1998; Hodzic et al., 2004; Malik et al., 2010) was tested by FRAP in HeLa cells using identical photobleaching conditions, e.g., laser intensity, bleach spot size, and measurement parameters. Nine of these were novel NETs identified by proteomics (Schirmer et al., 2003), while six were well-characterized NETs including two splice variants of lamina-associated polypeptide 1 (LAP1). Most of the characterized NETs had been analyzed by FRAP in different studies, though in some cases truncated proteins or different splice variants were used (Ellenberg et al., 1997; Ostlund et al., 1999; Rolls et al., 1999; Shimi et al., 2004; Goodchild and Dauer, 2005; detailed in Materials and methods). All proteins, except for SUN2, were fused to GFP at their C termini. The NETs had a wide range of physical characteristics such as size, isoelectric points, and numbers of membrane spans (Table I).

The $t_{1/2}$ merely indicates the time for 50% recovery of fluorescence after photobleaching and is used here as a relative measure of the protein mobility. The $t_{1/2}$s presented are means from at least eight individual experiments using multiple transfections (Fig. 1,

Published March 28, 2011

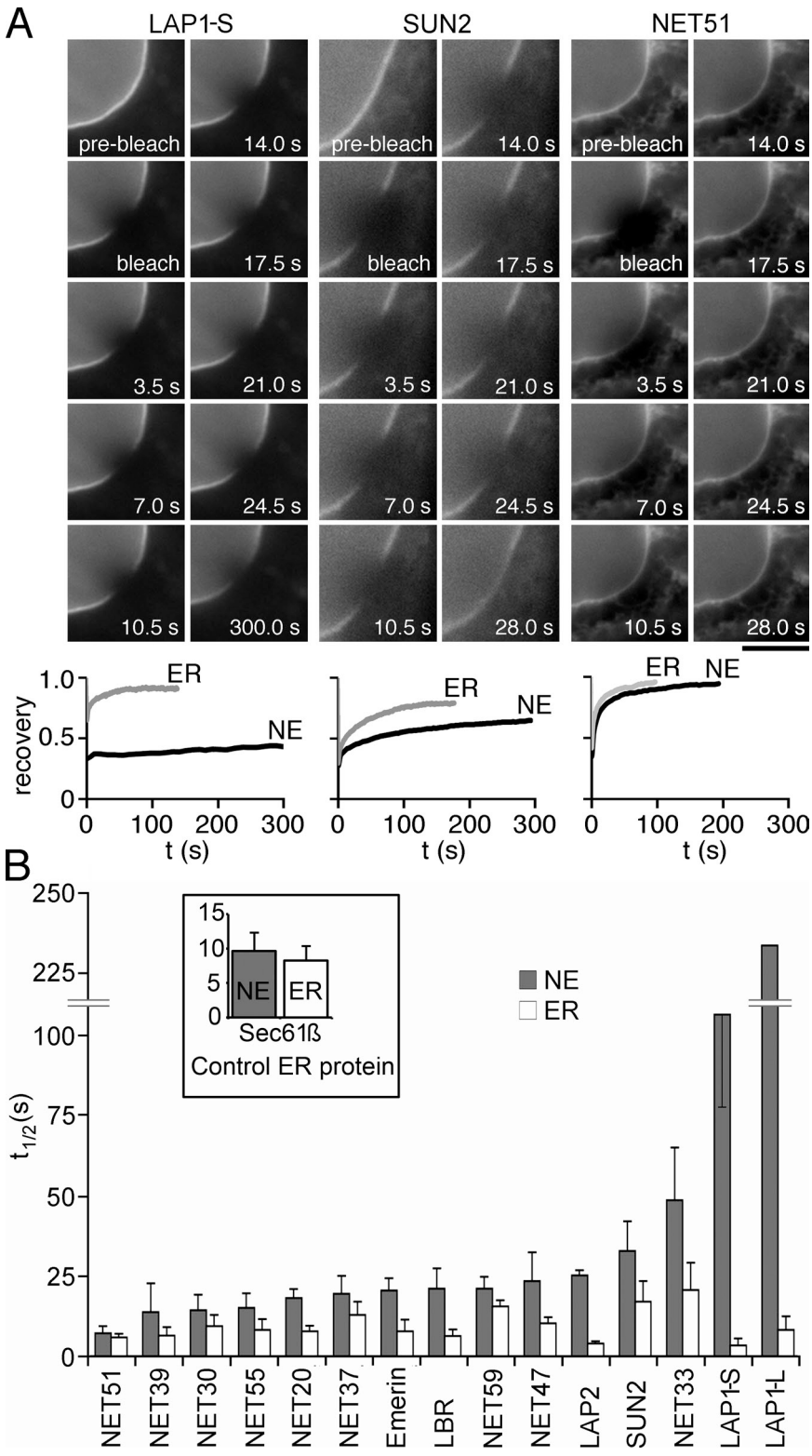

Figure 1. **FRAP of NETs reveals a wide range of mobilities.** (A) Images of NE FRAP for NETs with widely different $t_{1/2}$s. Bar, 10 µm. Graphs show fluorescence recovery kinetics in the NE and ER for the respective NETs, with normalized values plotted setting the prebleach to 1. (B) FRAP $t_{1/2}$s for all 15 NETs tested, calculated from normalized values. NE $t_{1/2}$s are shown in gray and ER $t_{1/2}$s in white. Error bars indicate SD based on at least eight independent experiments from multiple transfections. The $t_{1/2}$s and SD for LAP1-S is 105.7 ± 29.1 and LAP1-L is 233.5 ± 107.2. For all NETs, the $t_{1/2}$ in the ER was much smaller than the corresponding $t_{1/2}$ in the NE, and the range of $t_{1/2}$s in the ER was much narrower than the range in the NE. Inset shows $t_{1/2}$ of recovery for the control ER protein Sec61β. Virtually no difference is observed in the time of the ER and NE recovery for this protein, as NE recovery occurs almost exclusively in the ONM, which is continuous with the ER.

Fig. S1, and Table I). We observed a 30-fold range of $t_{1/2}$s among the new NETs tested here, whereas emerin and LAP2 $t_{1/2}$s were roughly similar to one another as described previously (Ostlund et al., 1999; Wu et al., 2002; Shimi et al., 2004). It is notable that some earlier studies differed in reported $t_{1/2}$s and mobile fractions for emerin, SUN2, and lamin B receptor (LBR; Ellenberg et al., 1997; Ostlund et al., 1999; Rolls et al., 1999), and we also observe minor differences from these earlier studies. These differences are probably caused by differences in the cell lines, constructs, and photobleach parameters used. This, however, could not account for the relative differences we observed across the wide range of NETs tested here, where all these parameters are constant. These differences also could not be caused by GFP photophysics because no recovery was observed in fixed samples (not depicted).

Published March 28, 2011

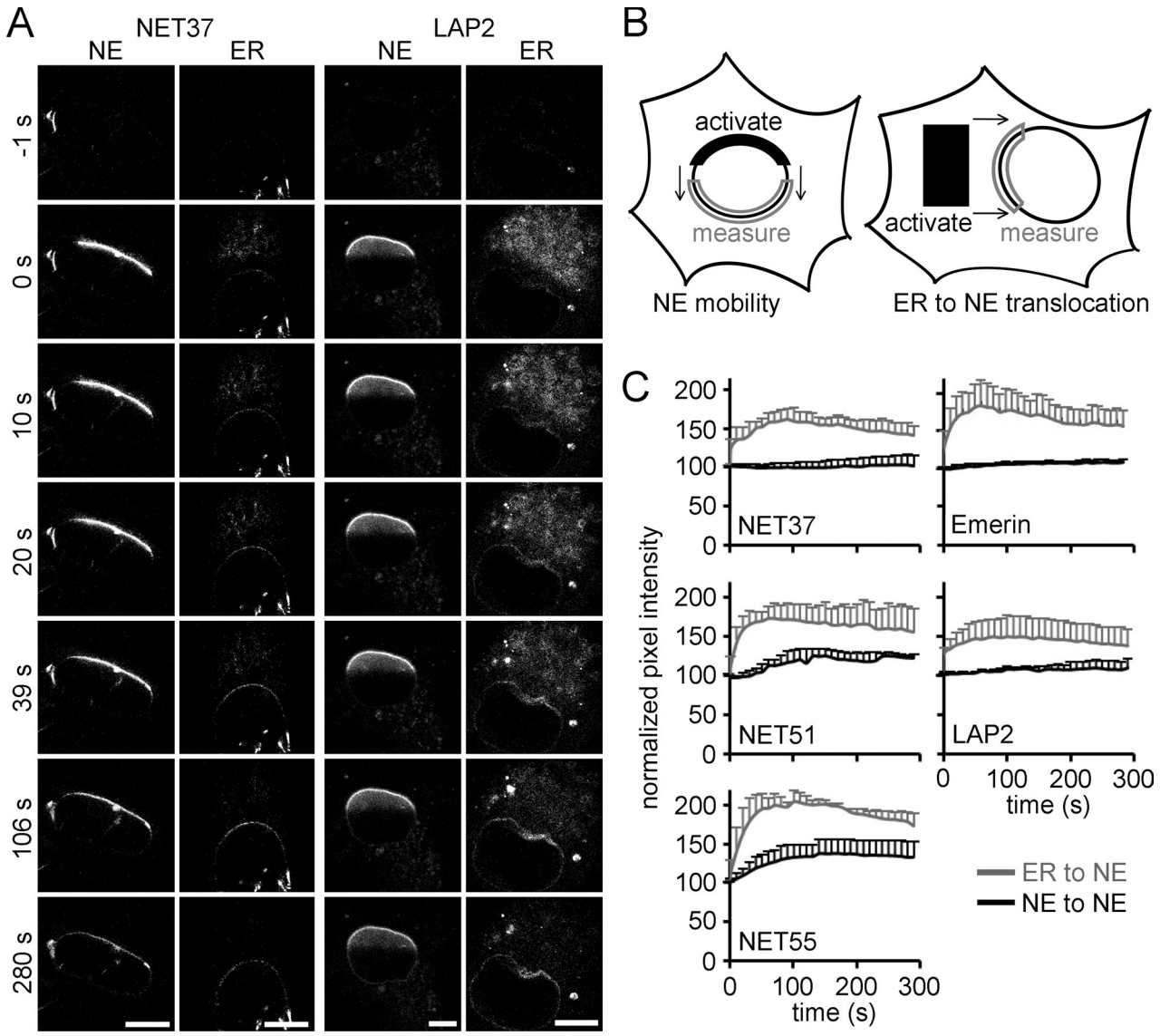

Figure 2. **PA distinguishes NE mobility from ER-NE mobility.** (A) Micrographs taken before and after PA at the time points shown on the left. NETs were photoactivated in the NE (left) and in the ER (right). After PA in the NE, the fluorescence signal remained largely stationary compared with PA in the ER, where fluorescence quickly distributed throughout the ER and accumulated at the NE. Bars, 5 µm. (B) Schematic of method for measurement of NE mobility and NE-to-ER translocation rates. Regions indicated were photoactivated and the fluorescence intensity in the gray boxes was measured over time. (C) Rates of mobility within the NE (black lines) were compared with rates of NE accumulation after PA in the ER (gray lines). The distance traveled by NETs was similar in both cases between the photoactivated region and the measured region, nonetheless NETs accumulated more rapidly in the NE when photoactivated in the ER, which confirms that translocation from the ER to the NE is faster than movement within the NE. Error bars show SD for 3–7 independent experiments using multiple transfections.

The mobility of each NET was also measured in the ER. A GFP fusion of the ER protein Sec61β served as a control. Any nuclear rim accumulation for Sec61β should derive from the ONM, which is continuous with the ER, because it is known to not accumulate in the INM; therefore, NE FRAP for Sec61β should roughly match ER FRAP, and this was observed (Fig. 1 B, inset). In contrast, FRAP $t_{1/2}$s measured for NETs were systematically and statistically significantly smaller in the ER than in the NE. If NETs with slow NE recovery (large $t_{1/2}$s) were also slow to recover in the ER, their large $t_{1/2}$s might reflect aggregation of the fusion protein; however, there was no correlation between NE and ER $t_{1/2}$s (Fig. 1 B). For example, LAP1-S had the second largest $t_{1/2}$ in the NE, yet had the smallest in the ER. Nonetheless, ER mobilities, though generally similar, were not all identical, which suggests that some NETs may have separate binding partners in the ER or an initial licensing step, as has been indicated for LBR (Braunagel et al., 2007). All NE and ER recovery curves as well as mobile fractions are given in Figs. S1 and S2.

FRAP is a cumulative measure of exchange within and between distinct NET populations

Five NETs with a wide range of FRAP $t_{1/2}$s were tested in PA experiments. When NETs were photoactivated in the NE (Fig. 2 A, left), most movement within the NE was very slow

Published March 28, 2011

Table II. **NE FRAP $t_{1/2}$s and estimated half-times for NE accumulation after PA in the ER or the NE**

NET	FRAP: NE $t_{1/2}$	PA: ER-to-NE $t_{1/2}$	PA: NE-to-NE $t_{1/2}$
	s	*s*	*s*
37	19.3 ± 5.5	27.8 ± 5.0	NA[a]
51	7.1 ± 2.2	7.0 ± 2.1	70.9 ± 32.2
55	14.9 ± 4.6	17.7 ± 9.0	47.6 ± 18.5
Emerin	20.3 ± 3.8	12.0 ± 4.2	56.8 ± 23.0
LAP2	25.0 ± 1.6	14.6 ± 6.1	70.2 ± 52.9

[a]NET37 exhibited too little movement in the NE after PA to measure a $t_{1/2}$.

compared with the recovery times measured by FRAP (Fig. 1). For example, although very little of photoactivated NET37 had dispersed even at 100 s, the NE FRAP $t_{1/2}$ for NET37 was 19 s. In contrast, PA in the ER resulted in very rapid dispersion of NETs throughout the ER and also rapid accumulation of NETs in the NE, as indicated by the appearance of discernible nuclear rim fluorescence (Fig. 2 A, right).

To better interpret PA results, the intensity of fluorescence on the opposite side of the nucleus from the photoactivated section was measured over time and plotted (Fig. 2 B). The accumulation of fluorescence in the NE was also calculated for NETs photoactivated in the ER to roughly determine the rate of movement from the ER to the NE. In all cases, the PA measurements for ER to NE movement were much smaller (i.e., faster) than those for movement within the NE (Fig. 2 C and Table II). Thus, much of the fluorescence recovery in the NE FRAP experiments likely comes from the protein exchanging between the ER and NE, whereas the dynamics of the measured fluorescence in the NE PA reflects both its redistribution within the NE and its loss to the ER.

Nonetheless, the relative contributions of the different populations to measured mobilities cannot be readily distinguished, and so we sought to model the exchange of protein between the populations. Another experimental measure needed for this is the mean relative abundance of each NET within the INM and ONM, as some of the measured FRAP recovery may occur in the ONM. Though all NETs analyzed here target to the INM (Senior and Gerace, 1988; Worman et al., 1988; Foisner and Gerace, 1993; Smith and Blobel, 1994; Squarzoni et al., 1998; Hodzic et al., 2004; Malik et al., 2010), their exogenous expression might saturate INM binding sites. Thus, most NET–GFP fusions were sampled by immunoelectron microscopy using antibodies to GFP. Though similarly overexpressed, the Sec61β–GFP fusion protein was almost entirely found in the ONM and the ER, whereas all NETs preferentially accumulated in the INM (Fig. 3).

As the majority of each NET accumulated in the INM and most recovery curves reached >80% of the prebleach levels, it would be impossible to achieve the measured fluorescence recoveries solely by recovery in the ONM. Therefore, some recovery must derive from protein newly translocated from the ER. The significant contribution of the translocation step to NET kinetics impacts on our ability to model these data. Because of the high complexity of this system, effective modeling could only be attempted on NETs that likely move by free diffusion as opposed to those using previously suggested ATP- and Ran-dependent translocation mechanisms (Ohba et al., 2004; King et al., 2006). Thus, we tested six NETs to determine how their mobility was affected by depletion of ATP or Ran.

Emerin and SUN2 mobility requires ATP

Though ATP and Ran were previously found to be important for translocation, neither study distinguished if these were separate requirements for different NETs or part of the same complex translocation mechanism (Ohba et al., 2004; King et al., 2006). To avoid pleiotropic effects of ATP depletion, cells were analyzed between 10 and 40 min after the depletion initiation. Within this short time window, no adverse affects of ATP depletion could be observed. Neither the measured $t_{1/2}$s nor the mobile fraction percentages of NET51, NET55, LAP2, or LBR were affected by ATP depletion (Fig. 4). In contrast, the emerin $t_{1/2}$ increased from 20.3 to 46.2 s, and its mobile fraction percentage decreased from 84 to 33% (Fig. 4 A). SUN2 was also affected by ATP depletion, with its mobile fraction percentage for NE FRAP dropping to <20%, making the $t_{1/2}$ unmeasurable. Thus, the previously described energy requirement (Ohba et al., 2004) only applies to a subset of INM proteins.

To test if the ATP requirement was caused by characteristics of the nucleoplasmic/cytoplasmic domain of emerin, this region (aa 1–224) was moved to the N terminus of NET51 and LBR. In both cases, the $t_{1/2}$ was increased after ATP depletion, similar to what was observed for wild-type (WT) emerin (Fig. 4 B). Thus, sequences required for the ATP-dependent step are in this region.

Emerin also has cytoplasmic partners (Cartegni et al., 1997; Lattanzi et al., 2000; Salpingidou et al., 2007), so its ER mobility was also retested with ATP depletion. Indeed, the ER mobility was also slower with ATP depletion (Fig. 4 C). Thus, the energy requirement may not pertain to the actual translocation step, but instead to a licensing step in the ER.

LBR requires Ran GTPase for translocation

The central channel nuclear transport factor Ran GTPase is also required for transport of two INM proteins in yeast (King et al., 2006). To test if Ran function is generally required for INM proteins, we used the Ran mutant Q69L that cannot hydrolyze GTP and dominant-negatively inhibits Ran function in vivo (Dickmanns et al., 1996; Silljé et al., 2006). Cells were cotransfected with NET–GFP constructs and a second plasmid encoding both untagged RanQ69L and an RFP reporter driven by separate promoters so that cells expressing the Ran mutant could be identified. Expression of the Ran mutant was confirmed

Published March 28, 2011

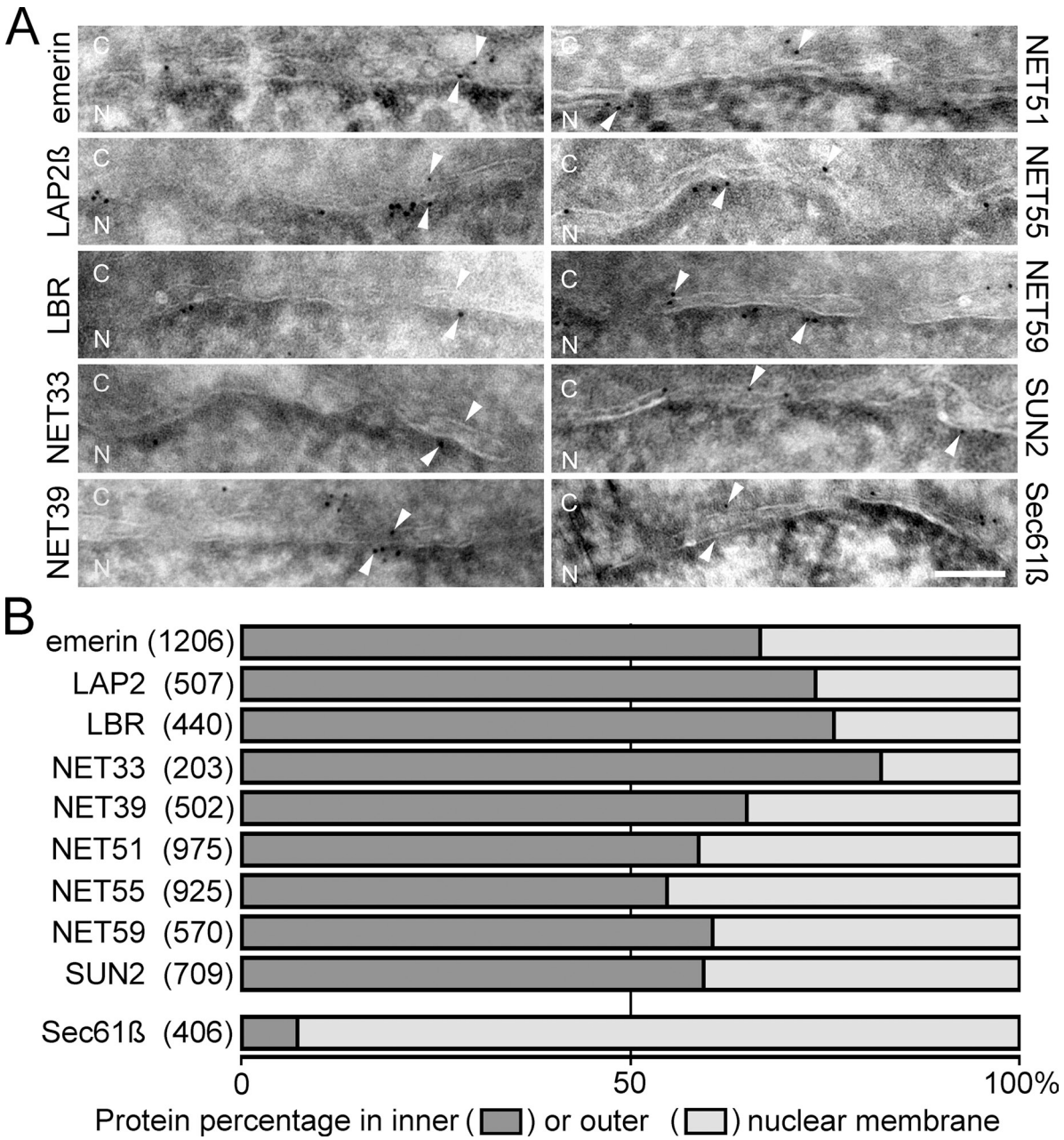

Figure 3. **Immunoelectron microscopy of exogenously expressed NET–GFP fusion proteins.** To measure accumulation in the ONM versus INM, NET–GFP fusions were transfected into HeLa cells and, after 24 h (the same as for FRAP experiments), were fixed and processed for immunoelectron microscopy. (A) Example micrographs are shown with 5-nm gold particles evident proximal to the double membrane of the NE. The cytoplasmic and nucleoplasmic faces are indicated by "C" and "N," respectively to identify the ONM and INM. Arrowheads point to a gold particle in the ONM (downward) and one in the INM (upwards). Bar, 100 nm. (B) For each NET INM and ONM, gold particles were counted (total particle number in parentheses) and the percentages in each membrane were plotted. Only ~5% of gold particles were in the INM for the Sec61β control, but for all NETs, gold particles were predominantly found in the INM.

by an increase in Ran levels both by immunoblotting and by immunofluorescence staining of matched cultures (Fig. 5 A). Cells were analyzed 24 h after transfection, at which point they were still healthy as assessed by morphology and membrane refraction, whereas by 2 d, deleterious secondary effects of Ran functional inhibition were evident. Of the six NETs tested, only LBR was affected by coexpression of the Ran mutant, nearly doubling its fluorescence recovery $t_{1/2}$ (Fig. 5 B). To test the possibility that NETs lacking a Ran effect use both Ran-dependent and ATP-dependent pathways redundantly, they were retested combining Ran functional inhibition with ATP depletion. The results were identical for the combined inhibition and the individual pathway inhibition (Fig. 5 B, bottom). Thus, the two pathways are separate and are not likely to function redundantly for the NETs that were unaffected by either alone.

For yeast NETs dependent on Ran, mutation of the single predicted NLSs blocked INM accumulation (King et al., 2006). Such an approach was impractical for human LBR because four separate NLSs were predicted using PSORTII (Nakai and Horton, 1999) so that their combined mutation would likely notably

Published March 28, 2011

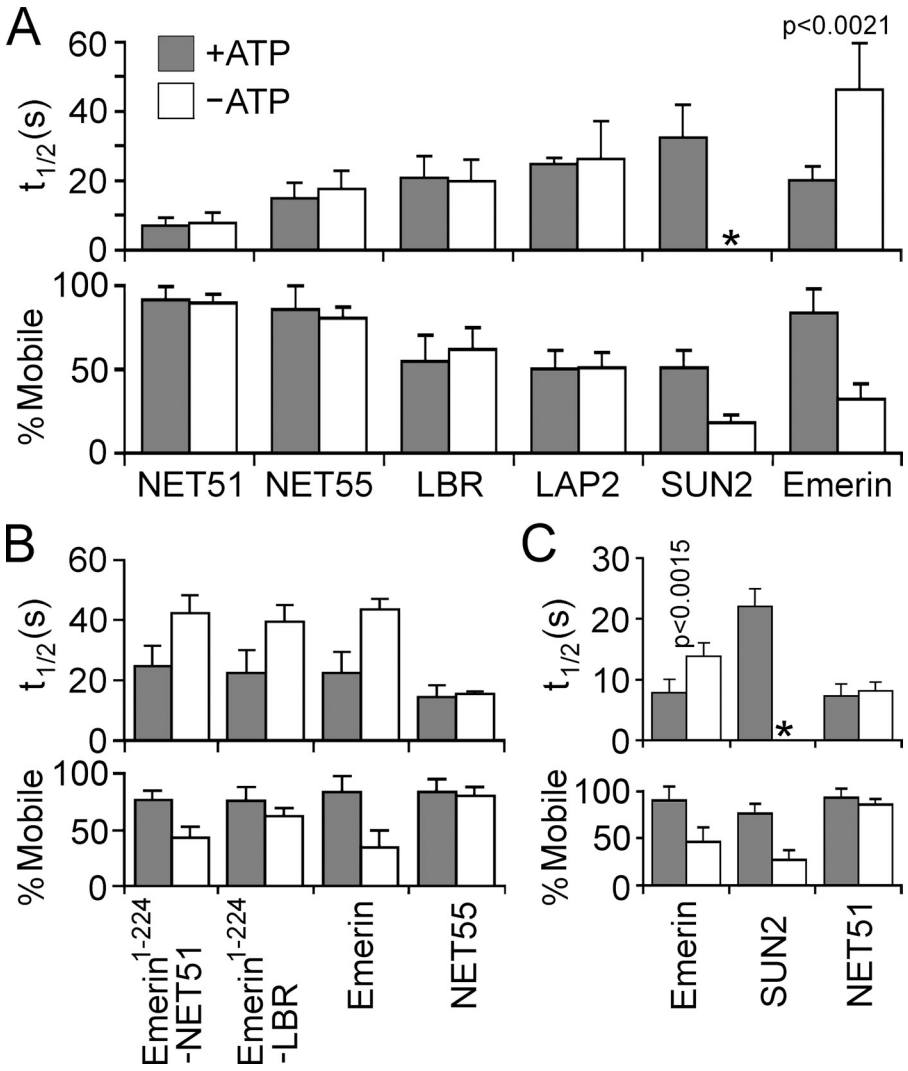

Figure 4. **Effect of ATP depletion on NET mobility.** NE FRAP in medium with an ATP depletion system or in the same medium without ATP depletion components. (A) The $t_{1/2}$s (top) and mobile percentages (bottom) were measured for six NETs. Emerin and SUN2 were strongly affected by ATP depletion. (B) The nucleoplasmic region of emerin (aa 1–224) was fused to NET51 and LBR, and these constructs were tested against WT emerin and NET55 as positive and negative controls. The emerin nucleoplasmic sequence conferred ATP dependence to NET51 and LBR. (C) ER FRAP was also tested with ATP depletion. Emerin and SUN2 mobility was also reduced in the ER upon ATP depletion. For SUN2, the mobile fraction was too low to make a certain $t_{1/2}$ calculation (asterisks). Error bars indicate SD from at least eight individual experiments.

alter protein structure. Thus, instead, the first 128 residues of LBR that include the three strongest predicted NLSs or the classical SV40 NLS (Goldfarb et al., 1986; Wychowski et al., 1986) were fused to three NETs with weak NLSs that had previously shown no Ran dependence: emerin, NET51, and NET55. This increased their NLS prediction scores, respectively, from 0.02, −0.22, and −0.47 to 1.44, 1.20, and 0.94 for the LBR NLSs and 1.76, 1.52, and 1.27 for the SV40 NLS (compared with 1.19 for WT LBR); however, it did not confer Ran dependence in any case (Fig. 5 C).

As it was possible that the NET–NLS fusions failed to become dependent on Ran because they have alternate mechanisms for INM translocation, an ER-resident protein Sec61β was also fused to the SV40 NLS. This resulted in its concentration at the NE and INM (Fig. 5 D) but failed to confer Ran dependence for the photobleach recovery as measured by $t_{1/2}$ (Fig. 5 E). Interestingly, the INM/ONM ratios of both NLS-Sec61β and LBR were not significantly altered by the Ran mutant (Fig. 5 F). The failure of RanQ69L to accumulate LBR in the ONM despite its doubling of the $t_{1/2}$ is likely caused by a high binding affinity for LBR in the INM (Worman et al., 1988; Ye and Worman, 1996) and the presence of alternate translocation pathways. Nonetheless, the effect of Ran is likely on the translocation step because the mutant had no effect on LBR FRAP in the ER or PA in the NE (Fig. S4).

A potential role for FGs in translocation

As NLSs did not appear to be responsible for Ran-dependent LBR translocation, we searched the LBR sequence for other characteristics relating to NPC functions. Strikingly, LBR has six FG pairs. This amino acid pairing is not common (only 1.5% of all human proteins have six or more FGs). FGs occur on both Nups and some transport receptors (e.g., importin/karyopherin-β with four FGs), and $FG^{receptor}$–FG^{nup} interactions have been proposed to facilitate translocation through the central channel of the NPC (Rexach and Blobel, 1995), although this has not been experimentally verified. Mutating all six FGs in LBR would likely disrupt structure, so to test a role for FGs, a short sequence of four FGs (underlined) "MFGHTFGFGQSVFG" was fused to the N-terminus of NET51 and NET55. These were tested in the presence or absence of RanQ69L, but no effect of the Ran mutant was observed (Fig. 6 A). Though addition of FGs failed to confer Ran dependence, interestingly, the constructs carrying the four FGs had faster recoveries than their WT counterparts (Fig. 6 B).

Published March 28, 2011

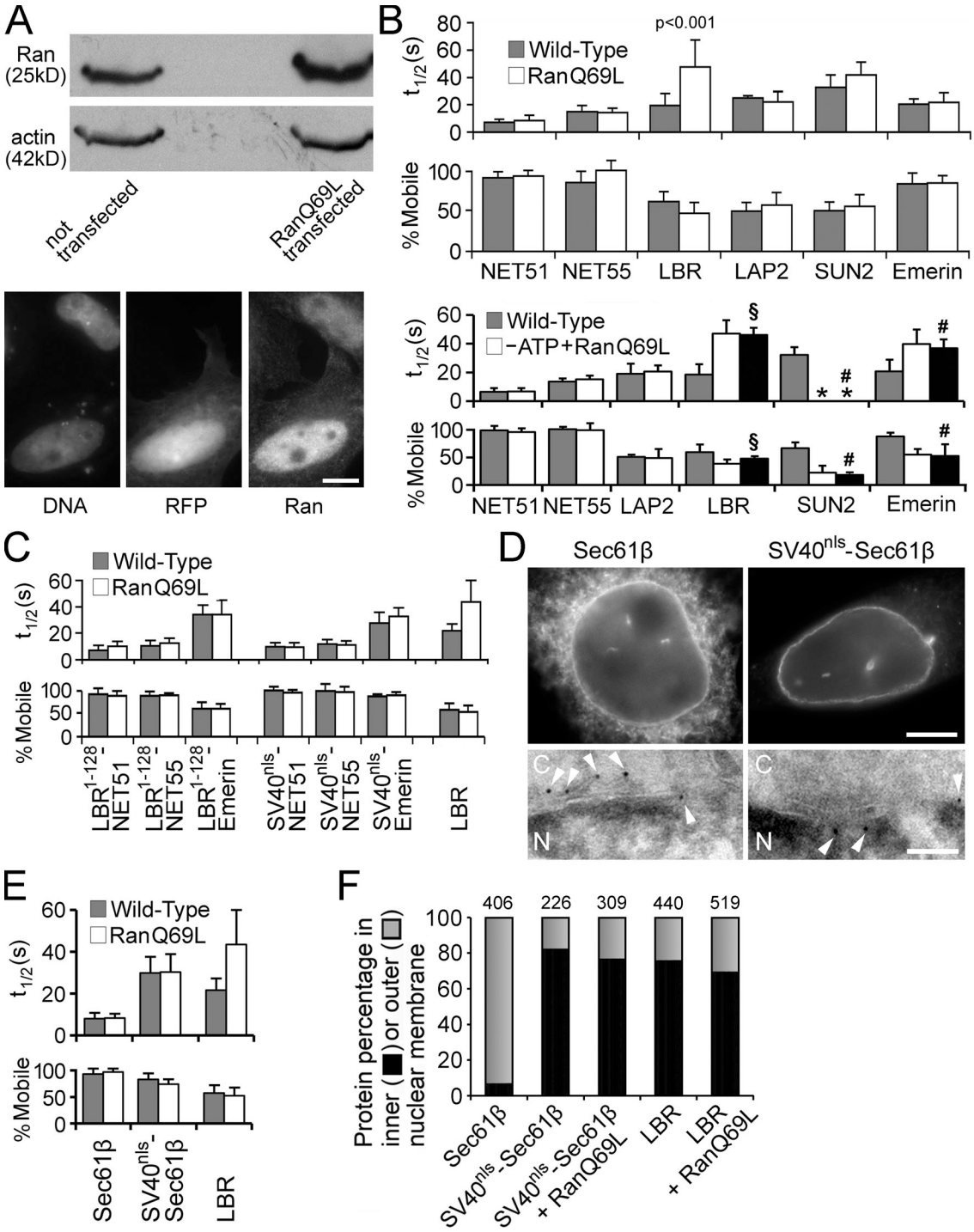

Figure 5. **Inhibition of the Ran-GTPase interferes with LBR translocation.** Cells were cotransfected with NETs and the Q69L dominant-negative Ran mutant. (A) Confirmation of RanQ69L expression. Because Ran function is sensitive to epitope tags, untagged RanQ69L was expressed from a plasmid that separately expressed mRFP. The immunoblot shows increased total Ran levels in the transfected cells (actin is a loading control). Immunofluorescence images show a transfected cell indicated by mRFP signal that also exhibits an increase in staining with Ran antibodies. (B) The $t_{1/2}$s (top) and the protein mobile percentages (bottom) were measured for NETs and plotted. Only LBR was inhibited by Ran functional depletion. In the lower panels, cells were subjected to a combination of ATP depletion and the Ran mutant. Black bars are the values for RanQ69L alone (§) or ATP depletion alone (#) for comparison. (C) The region of LBR containing its three strongest predicted nuclear localization signals (aa 1–128) or the SV40 NLS was fused to the N terminus of full-length NET51, NET55, and emerin. FRAP experiments were again performed in the presence or absence of the Ran mutant. The added NLSs failed to confer Ran dependence. (D) Addition of the SV40 NLS to the ER protein Sec61β causes its INM accumulation, as indicated by significant reduction of ER fluorescence (top) and immunoelectron microscopy (bottom). Cytoplasmic (C) and nucleoplasmic (N) sides of the nuclear membrane are marked and ONM gold particles are highlighted with downward arrowheads while INM particles are highlighted with upwards arrowheads. (E) The Ran mutant had no effect on the $t_{1/2}$s or mobile fractions for either Sec61β or NLS-Sec61β. (F) The percentages of Sec61β, NLS-Sec61β, and LBR distributed between ONM and INM in the absence or presence of RanQ69L are graphed. The total number of gold particles counted is listed above the bars. All error bars indicate SD from at least eight individual experiments. Bars: (A and D, top) 5 µm; (D, bottom) 100 nm.

Published March 28, 2011

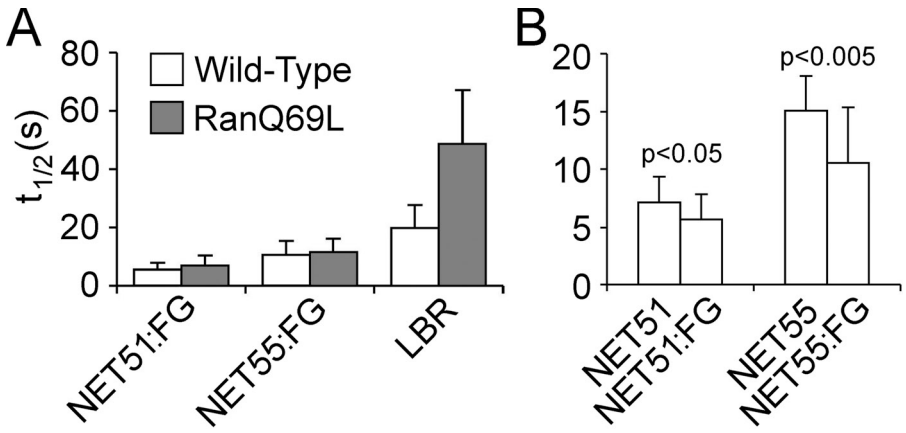

Figure 6. **Effect of FG motifs on NET mobilities.** (A) A sequence containing multiple FG motifs (underlined) "MFGHTFGFGQSVFG" was fused to the N terminus of NET51 and NET55 and tested in the presence or absence of RanQ69L. The addition of the FG motifs also failed to confer Ran dependence to the NETs, with LBR serving as a positive control. (B) Comparison of the FG motif–containing constructs and WT NETs without the Ran mutant revealed that addition of the FGs facilitated translocation. Error bars indicate SD from at least eight individual experiments.

This finding is particularly intriguing in light of the significant enrichment of FGs in NETs compared with other proteins. A set of 199 total predicted NETs from a rat liver NE proteomics dataset (Schirmer et al., 2003) were compared with the total predicted transmembrane proteins encoded in the rat genome. Because some FGs might be embedded in the lipid bilayer, the predicted membrane spans were removed from the amino acid sequences. The number of remaining FGs was then calculated for each protein and plotted as a percentage of the total proteins in each dataset with the number of FGs ≥ *n* (Fig. 7 A). As the number of FGs per protein increased on the x axis, the enrichment of FGs in NETs compared with general transmembrane proteins increased. When considering transmembrane proteins with 14 or more FGs, the percentage among NETs was >40-fold higher than in the set of transmembrane proteins from the whole genome. When comparing NETs to just mitochondrial transmembrane proteins (extracted from Mootha et al., 2003), the NET enrichment in FGs had a P-value of 4.77×10^{-5} (Fig. 7 B).

The enrichment for FGs is the more striking in its contrast with the lack of predicted NLSs. Nearly 80% of the liver NETs had NLS prediction scores below zero. The median NLS prediction score among NETs was well below that of the soluble proteins found in the same liver NE proteomics datasets (Fig. 7 C).

Finally, analysis of this set of liver NETs supports the hypothesis that INM proteins translocate through the peripheral channels of the NPCs because the size distribution for nucleoplasmic/cytoplasmic and lumenal amino acid residues revealed a striking limitation on nucleoplasmic mass below the 60-kD cutoff for peripheral channel translocation (Fig. 7 D). In contrast, lumenal mass covered a wide range with ∼25% of NETS exceeding the exclusion limit. The few outliers for nucleoplasmic/cytoplasmic mass are likely ONM proteins or result from mispredicted topologies. In contrast to this NET dataset, mitochondrial transmembrane proteins (Mootha et al., 2003) had very similar median values for cytoplasmic/inner and lumenal/outer mass (Fig. 7 E).

Nup35 facilitates Ran-mediated INM translocation

The ability of FGs to decrease FRAP $t_{1/2}$s suggested the possibility that the NETs interact with FG-Nups during translocation. Recent NPC structural refinements indicate that some FG-Nups reside in the peripheral channels, among which is Nup35 (Nup53p in yeast; Alber et al., 2007). As Nup35 depletion in vertebrate cells yields no loss in cell viability (Hawryluk-Gara et al., 2005), NETs were retested in cells depleted for Nup35 by siRNA to determine if it contributes to INM translocation (Fig. 8 A). Nup35 protein levels were significantly reduced (Fig. 8 B), but no significant difference in NET translocation was observed between WT and Nup35-depleted cells except in the case of LBR ($P < 0.0003$). The fact that most NETs were unaffected by Nup35 depletion indicates that the effect on LBR is specific and does not result from NPC structural changes that create a steric block to translocation.

To test if the LBR Ran effect is synergistic with the LBR Nup35 effect, the Nup35 knockdown was tested in combination with RanQ69L (Fig. 8 C). Loss of Nup35 increased the $t_{1/2}$ for LBR to levels similar to those observed with the RanQ69L mutant. The effect on LBR from the combination of Nup35 depletion and Ran inhibition was similar to either alone. Thus, the Ran functional-depletion effect on LBR requires a positive function of Nup35.

Separately, the FG-NET51 was compared with WT NET51 in the presence or absence of Nup35 depletion. (FG-NET55 was not tested because NET55 has four FGs without the added sequence and so cannot effectively serve as a negative control.) The $t_{1/2}$ for WT NET51 was not affected by Nup35 depletion, but the $t_{1/2}$ for FG-NET51 was increased significantly (Fig. 8 D). Thus, Nup35 appears to play separate roles in Ran-mediated and FG-mediated INM protein translocation.

A simple biophysical model for the dynamics of NETs

To gain more quantitative insight into the relative contribution of various processes affecting the mobility of NETs, we sought to interpret our experimental data using a simple biophysical model for NETs that translocate by unaided diffusion (see Materials and methods for details). LAP2, LAP1-L, and NET55 were analyzed because they exhibit a broad range of FRAP $t_{1/2}$s and appear to be independent of active transport mechanisms (Table III). An average HeLa nucleus has a volume of ∼1,000 μm^3, with a corresponding surface area of ∼500 μm^2. Estimating 2,770 NPCs/nucleus (Ribbeck and Görlich, 2001;

Published March 28, 2011

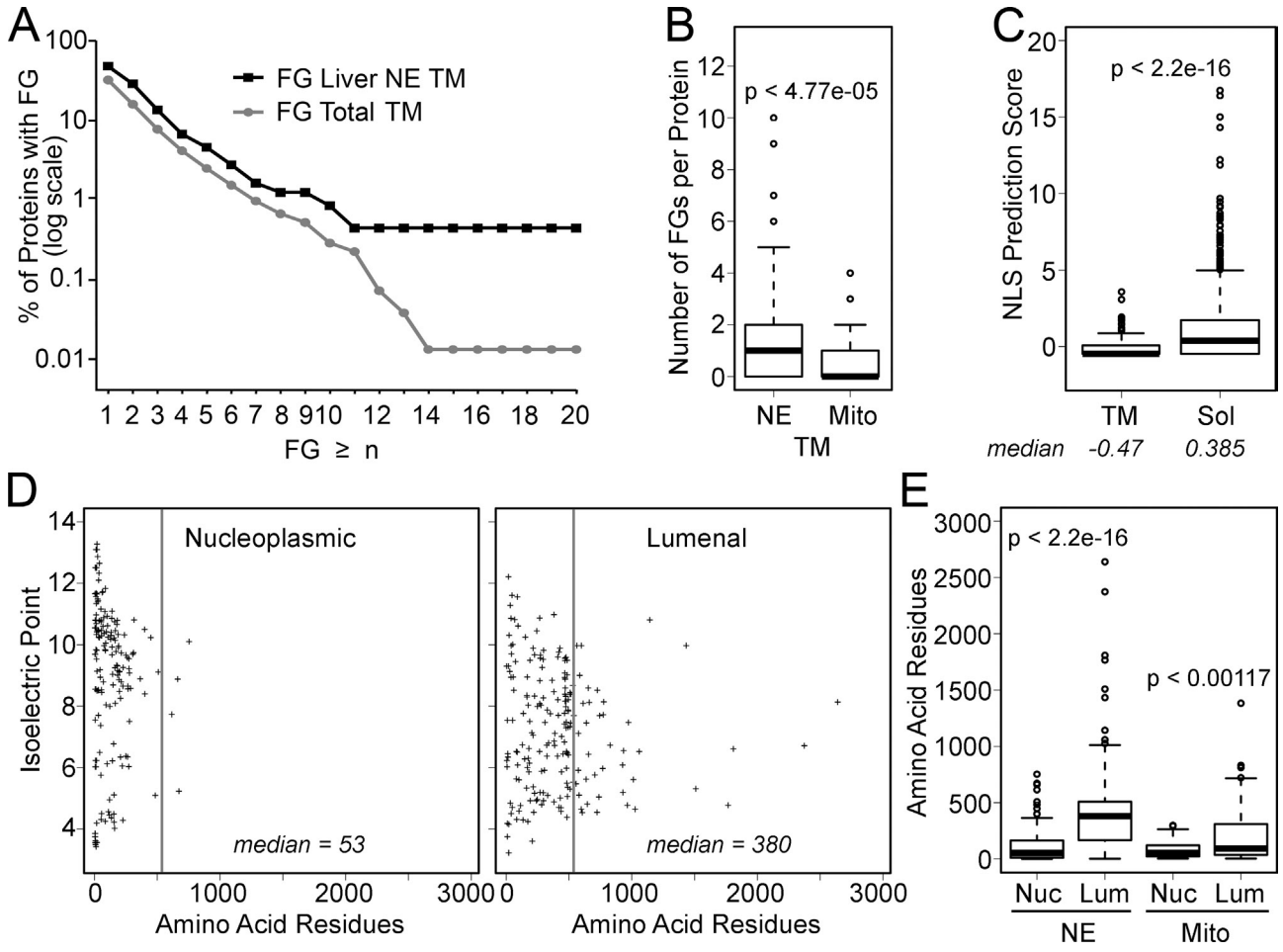

Figure 7. **FGs are enriched in NETs.** Analysis of a dataset of 199 predicted NETs identified by proteomics of liver NEs revealed shared characteristics consistent with the findings described here. A list of mitochondrial proteins separately identified by proteomics served as a control. In all cases, the hypothesis that two sets were different was tested using the Kolmogorov-Smirnov test to generate listed P-values. These are also given along with D-values in Table S2. (A) To determine FG sequences that could potentially interact with Nups, NET sequences minus their predicted transmembrane-spanning segments were compared with all predicted transmembrane proteins coded by the rat genome similarly modified. The percentage of total proteins in each set that had "*n*" or more FGs was plotted using a logarithmic scale. (B) The data generated from the analysis in A are plotted using Tukey's box plots, but comparing the NETs to mitochondrial proteins. Very few FGs were observed in mitochondrial transmembrane proteins compared with NETs. (C) The scores for NLS predictions of NETs (TM) and soluble (Sol) NE proteins are plotted using Tukey's box plots. The median NLS score is <0 for the NETs. (D) The predicted sizes and isoelectric points of lumenal and nucleoplasmic sequences were calculated and plotted. A gray line marks the predicted size limit of the peripheral channels of the NPC. Nucleoplasmic sequences tended to be much smaller and more basic than lumenal sequences. (E) The values for rodent liver NETs and mouse mitochondrial proteins were plotted using Tukey's box plots with median (central line), two quartiles above and below (box), and third quartile (error bars) shown. A large difference in the median value for the number of amino acid residues is observed between nucleoplasmic (Nuc) and lumenal (Lum) populations for the NETs, but mitochondrial transmembrane proteins exhibit similar median values between the two populations.

Maeshima et al., 2010), the NPCs should be situated ∼425 nm apart. Thus, a freely diffusing protein with the diffusion coefficient ∼0.1 μm^2/s should reach an NPC in <1 s in either the ONM or INM. Given this negligible time, the model approximates NPC translocation as a spatially homogeneous reversible first-order reaction with identical rates for both directions. As LAP1 and LAP2 and many other NETs bind lamins (Senior and Gerace, 1988; Worman et al., 1988; Foisner and Gerace, 1993; Clements et al., 2000; Sakaki et al., 2001; Mattout-Drubezki and Gruenbaum, 2003; Hodzic et al., 2004; Schirmer and Foisner, 2007), we further assumed the existence of immotile binding sites in the INM that effectively trap the NETs. Under these assumptions, a NET can be associated with one of the three NE pools: (1) free protein in the ONM and ER, (2) free protein in the INM, and (3) protein bound to immobile sites in the INM.

We first calculated ER diffusion coefficients from our ER FRAP data assuming these proteins lack binding partners in the ER. Stringent analysis of ER diffusion is a complex computational problem because of the 3D structure of cisterns and curved tubes (Sbalzarini et al., 2005, 2006). Nevertheless, its spatial ubiquity and compactness enables its simplified treatment as a continuous 2D sheet with no more than twofold underestimation of the true diffusion coefficients (Sbalzarini et al., 2006). All NET ER diffusion coefficients were found in the range of 0.01–0.1 μm^2/s (see Table III). We next analyzed the NE FRAP data. Although model complexity was reduced to the absolute minimum with only four kinetic parameters (NPC translocation rate, retention trap concentration, and on and off binding rates) in addition to the protein diffusion coefficient, we could fit different sets of parameters when considering just

Published March 28, 2011

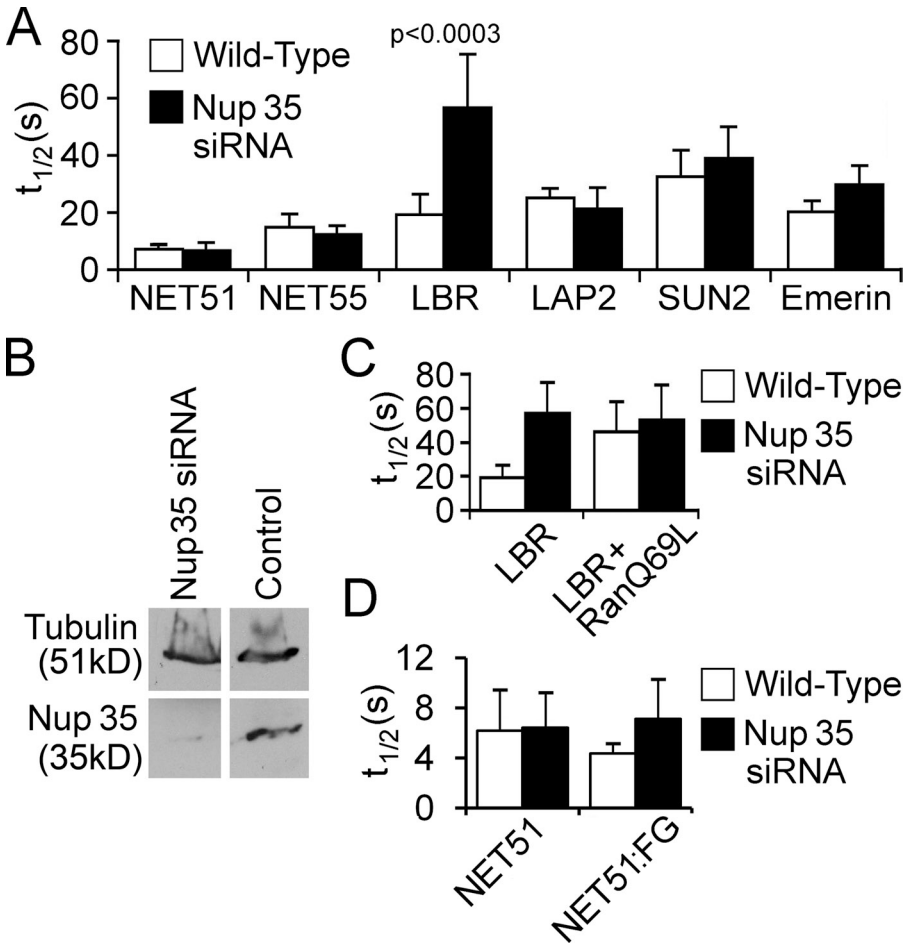

Figure 8. **Effect of Nup35 knockdown on NET translocation.** Levels of the nucleoporin Nup35 (Nup53p in yeast) were depleted by RNAi. (A) The $t_{1/2}$s were measured for NETs in WT cells and cells knocked down for Nup35. Only LBR translocation was affected by the loss of Nup35. (B) Confirmation of Nup35 knockdown by immunoblotting with Nup35 antibodies using tubulin as a loading control. Cells were lysed to measure protein levels 48 h after transfection. (C) The $t_{1/2}$s were measured for LBR in the presence or absence of the RanQ69L mutant and in the presence or absence of the Nup35 knockdown. Inhibition was similar for the Nup35 knockdown and the Ran functional depletion, and both together were not increased. (D) WT NET51 was compared with NET51 carrying four additional FGs (WT NET51 has one FG, but it is within a membrane span) with or without Nup35 knockdown. The increased mobility conferred by the FGs is lost in the absence of Nup35. Error bars indicate SD from at least eight individual experiments.

the measured FRAP kinetics. However, combining FRAP and PA data allowed us to reliably constrain the two most important characteristics: the half-lives corresponding to the NPC translocation and retention traps. Re-measuring FRAP dynamics over longer times provided reliable estimates for the binding off-rates (half-life ~0.7/off-rate). Using these values, the NPC translocation half-lives were computed from the corresponding PA curves. The best fit to the FRAP and PA data were achieved with the NET diffusion coefficients slightly higher than values inferred from the ER FRAP data (Table III), which is consistent with previous results (Sbalzarini et al., 2006).

This model-based analysis indicated that, despite their widely divergent FRAP $t_{1/2}$s, all three NETs possessed similar ONM–INM translocation times of ~1 min, which is consistent with the existence of an efficient translocation mechanism associated with free diffusion through the NPC peripheral channels. Apart from NET55 that showed only a moderate preference for the INM, the binding half-lives of the other NETs were found to be at least an order of magnitude longer than the ONM–INM translocation time. The difference in the FRAP dynamics between LAP2 and LAP1-L can be accounted for by the different effective concentration of binding sites in the INM rather than from different off-rates. Although we cannot reliably calculate the absolute concentrations of binding sites (they are defined in relation to the unknown steady-state concentration of the free protein), this result is consistent with our EM data and earlier published data on the ONM/INM distribution of LAP1-L (Senior and Gerace, 1988) that together indicate a higher preference for LAP1-L rather than LAP2 for the INM. Cumulatively, the results of our modeling suggest that the observed wide spread of FRAP $t_{1/2}$s between the proteins unaffected by Ran or ATP depletion can be explained by their different modes of interaction in the INM rather than by varied times necessary to traverse the NPC, which is consistent with free diffusion.

Table III. **Parameters of ER-NE protein dynamics estimated using modeling-based analysis**

NET	$t_{1/2}$	*D* in ER	*D* in NE	ONM/INM ratio	$t_{1/2}$, INM binding	$t_{1/2}$, NPC translocation
		$\mu m^2/s$	$\mu m^2/s$			*s*
NET55	14.9	0.01–0.03	0.05–0.07	45:55	90–110 s	50–70
LAP2	25	0.05–0.1	0.05–0.1	30:70	8–12 min	60–80
LAP1L	233	0.05–0.07	0.08–0.1	05:95[a]	9–14 min	70–140

[a]Inferred from the model, all others were calculated.

Published March 28, 2011

Discussion

Although existing technologies are insufficient to perfectly resolve each step in a NET's journey from its synthesis in the ER to accumulation in the INM, our systematic analysis of a representative panel of NETs has revealed many crucial steps and requirements. First, different subsets of NETs have distinct requirements for energy and classical transport proteins (Ohba et al., 2004; King et al., 2006; Saksena et al., 2006), which are independent of one another. Second, the finding that FGs can speed the half-times of recovery suggests a novel mechanism to facilitate the translocation step. Third, the effect of Nup35 knockdown on NET mobility and size limitation within the larger set of NETs strengthens earlier studies (Powell and Burke, 1990; Soullam and Worman, 1993, 1995) arguing for translocation through the NPC peripheral channels. Fourth, expanding on the original lateral diffusion–retention hypothesis, NET tethering in the INM is a major contributor to the differences observed between NET FRAP half-times. The combination of FRAP and PA approaches supported by model-based analysis of the resulting data has yielded significant progress in resolving the various steps in NET translocation and mobility.

The absence of Ran inhibition or ATP depletion effects on half of the NETs tested here suggests that many NETs translocate by unregulated lateral diffusion. The rapid NE accumulation in our ER PA studies and modeling is also consistent with this, as the ONM–INM exchange step had similar kinetics for all three NETs. Nonetheless, we cannot rule out the possibility of additional regulated translocation mechanisms involving different NPC components for other NETs. In yeast, Nup170 was required for INM accumulation of Heh2 (King et al., 2006), whereas it was not required for INM accumulation of Doa10 (Deng and Hochstrasser, 2006). In frogs, a role was found for Nup188 (Theerthagiri et al., 2010), whereas in human cells, antibodies to gp210 blocked NET translocation (Ohba et al., 2004), and we found that knockdown of Nup35 slowed NET mobility. The finding of so many Nups with effects on NET translocation would be surprising if a specific role for each Nup was required. More likely it indicates differences in the structure of the NPC between the organisms used or that effects are caused by the general disruption of the NPC structure.

The dependence of LBR mobility/translocation on functional Ran GTPase is consistent with two previous studies indicating LBR interactions with classical NPC components and a possible licensing step (Braunagel et al., 2007; Ma et al., 2007). However, in contrast to the yeast system, where mutating the NET NLSs blocked translocation (King et al., 2006), we find that addition of SV40 or LBR NLSs to other NETs failed to confer Ran dependence. Moreover, several NETs had NLSs (Table I) but exhibited no Ran dependence. As many INM proteins bind chromatin and have basic isoelectric points (Ulbert et al., 2006), it is possible that these characteristics result in erroneous predictions of classical basic NLSs. This tendency toward higher isoelectric points is confirmed from our larger collection of putative and confirmed NETs identified by proteomics. Another possibility is that the NLSs are redundant with other exchange mechanisms. SUN2 was recently reported to have an NLS that binds importin α/β in a Ran-dependent manner, but mutation of this NLS did not impair SUN2 targeting in interphase cells (Turgay et al., 2010). This is consistent with our results that SUN2 mobility was unaffected by Ran functional depletion.

The striking size limitation observed in larger datasets and the finding that both Ran-dependent and FG-facilitated mechanisms are affected by Nup35 depletion support the involvement of the NPC peripheral channels. Though NPC reconstruction supports a position for yeast Nup35 (Nup53p) internally within the peripheral channels (Alber et al., 2007) while another study argues that, in vertebrates, Nup35 binds lamins toward the nucleoplasmic face (Hawryluk-Gara et al., 2005), both studies are consistent with Nup35 being associated with the peripheral rather than central channels. The earlier finding that yeast Nup35 (Nup53p) interacts with the import receptor kap121p (Marelli et al., 1998) is consistent with Nup35 involvement in the Ran-dependent mechanism. Although it remains unclear whether FGs on some transport receptors actually interact with FGs on Nups during translocation, our finding that adding FGs to NET51 affected its FRAP mobility in a Nup35-dependent manner is consistent with this hypothesis (Rexach and Blobel, 1995). In this case, FGs on NETs might act as their own transport receptors. This model is the more attractive because NETs that approach the ∼60-kD diffusion limit of the peripheral channels could not afford the added mass from a transport receptor, and thus such proteins would benefit from being able to directly interact with FG-Nups.

Materials and methods

Plasmid construction

Human NETs (or rat LAP1/2) were cloned into the pEGFP-N vector series (Takara Bio Inc.) except for SUN2 in pEGFP-C3 (a gift of D. Hodzic, Washington University School of Medicine, St Louis, MO; Hodzic et al., 2004), yielding linkers ranging from 7 to 23 amino acids. Notably, earlier studies on LBR used a fragment (Ellenberg et al., 1997; Rolls et al., 1999) where we used the entire protein. Also, the two rat splice variants of LAP1 we tested (Martin et al., 1995) both differ from the mouse one previously tested by FRAP (Goodchild and Dauer, 2005). Sec61β–GFP was a gift of T. Rapoport (Howard Hughes Medical Institute, Harvard Medical School, Boston, MA). As this study was initiated before we became aware of the specific monomeric GFP, LAP2, NET51, and NET55 were retested using the specific monomeric GFP, yielding no significant differences in results. For photoactivatable constructs, NETs were inserted into pPA-GFP-C1, leaving a linker of 6 aa in all cases (Patterson and Lippincott-Schwartz, 2002). Primers encoding the SV40 NLS "MGTAGTPPKKKRKVEDPG" or the added FGs (underlined) "MFGHTFGFGQSVFG" were inserted at the 5′ end of full-length NET51, NET55, and/or emerin cDNAs in pEGFP-N2.

Transfection and cell culture

HeLa cells were grown in DME supplemented with 10% fetal calf serum, 100 U/ml penicillin, and 100 mg/ml streptomycin. Cells were plated onto 25-mm coverslips in 35-mm dishes and transfected at 20% confluency with 0.5 µg of reporter using Fugene HD (Roche).

PA experiments

A confocal system (SP5; Leica) equipped with a 60× 1.4 NA objective lens and 405 nm UV laser were used for GFP PA. Cells were cotransfected with NET20 fused to mRFP so that the NE and ER could be viewed to determine the region for PA. NET20 was used because it was extractible with Triton X-100 and thus unlikely to interact with other NETs or lamina components. Cells were first placed in a heated chamber in complete DME medium at 37°C. Then a region was selected based on the NET20-mRFP, the selected region was photoactivated at 8% laser power, and recovery of fluorescence

Published March 28, 2011

was measured by scanning the whole cell at low power every 10 s. Experiments for calculating diffusion coefficients were performed using similarly sized regions for the activation in the ER. For activation in the NE, a region representing 30–50% of the circumference of the nuclear rim was carefully marked so as to minimize any coactivation in the ER. Data were collected using the SP5 FRAP application suite (Leica). Data were then processed with Image-Pro Plus Analyzer 7 (Media Cybernetics).

FRAP experiments

All FRAP experiments for regular EGFP constructs were performed on a wide-field DeltaVision microscope (Applied Precision; IX70 microscope [Olympus] and CoolSNAP HQ camera [Photometrics]) with an attached 488 nm laser using a 60× Plan-Apochromat oil 1.4 NA objective lens. HeLa cells were analyzed at 15–20 h after transfection unless otherwise stated using a 37°C heated chamber with complete DME medium containing 25 mM Hepes-KOH. Five prebleach images were taken followed by bleaching a spot of 5.7 μm^2 for 1 s at full laser intensity so that between 20 and 40% fluorescence intensity was retained. Fluorescence recovery was measured every 3.5 s. Data were collected using the SoftWoRx software v. 3.5 and processed with Image-Pro Plus Analyzer 6 (Media Cybernetics). Intensity measurements and $t_{1/2}$ calculations were made using a macro written in Visual Basic within Image Pro according to Phair and Misteli (2001). In brief, a region of interest was applied to the whole cell, the bleach area, and the background. The region of interest was applied to each frame in the FRAP sequence, automatically correcting for photobleaching compared with five prebleach images. Movement of the bleach area because of cell movement was corrected by applying any change in the center xy position of the whole cell to the position of the bleach area. Any cell exhibiting rotational changes of position was discarded or measured manually. The $t_{1/2}$s were calculated using normalized fluorescence values, setting the immediate postbleach value to zero and the mean of the last 10 points of the recovery curves to 100.

Immunoelectron microscopy

Immunoelectron microscopy was performed on HeLa cells transiently transfected with different NETs fused to GFP. Cells were fixed in 4% paraformaldehyde, pelleted, and infiltrated with 2.3 M sucrose, then frozen by plunging into liquid nitrogen. Frozen pellets were sectioned on a cryo-ultramicrotome (UC6 with FC6 cryo-attachment; Leica). Cryosections were thawed, rinsed in PBS with 1% glycine, incubated in PBS with 1% BSA, incubated with rabbit anti-GFP antibody (Abcam) at 1:400 dilution, and rinsed in PBS, then incubated with the secondary anti–rabbit IgG antibody conjugated to 5 nm colloidal gold (Agar Scientific). Grids were then rinsed in PBS, transferred to 1% glutaraldehyde (Agar Scientific) in PBS, washed in water, and embedded in 2% methyl cellulose containing 0.4% uranyl acetate (Agar Scientific). Images were taken on an electron microscope (H7600; Hitachi) at 100 kV and at a magnification of 80,000–100,000.

Nup35 knockdown with siRNA

Knockdown of Nup35 was effected using an oligo (Eurogentec) designed to target 5′-UGCCCAGUUCUUACCUGGA-3′ of the human Nup35 mRNA. Cells were used for experiments 48–60 h after nucleofection of 7 µg of the oligo per million cells using kit R (Lonza). Polyclonal antibodies to detect Nup35 protein were obtained from Tebu-bio (157H00129401-B01).

ATP depletion experiments

ATP depletion experiments were performed as in Ohba et al. (2004). In brief, 10 min before FRAP analysis, the medium was changed to glucose-free medium containing 10 mM sodium azide, 6 mM 2-deoxyglucose, 25 mM Hepes-KOH, and 10% FBS. Cells were discarded after 40 min to reduce the possibility of secondary effects of ATP depletion influencing FRAP results.

Ran depletion experiments

To inhibit Ran function, a plasmid was constructed carrying the untagged human Ran gene containing the Q69L mutation behind the cytomegalovirus (CMV) promoter and separately expressing monomeric RFP (Campbell et al., 2002) driven by a separate CMV promoter. This construct was cotransfected with NET–GFP fusions and cells were analyzed after 24 h. The increase in Ran levels was confirmed with purified mouse monoclonal anti–human Ran antibody 610341 (BD).

Bioinformatic analysis

Predicted NETs and soluble proteins were extracted from rodent liver NE proteomic datasets (Schirmer et al., 2003). The NET dataset included 199 novel and previously characterized transmembrane proteins. Mitochondrial proteins were extracted from a proteomic study of mouse mitochondria (Mootha et al., 2003). Transmembrane segments were removed from NETs and the nucleoplasmic and luminal sequences were separated based on TMHMM v2.0 predictions of membrane topology (Krogh et al., 2001). The number of amino acid residues and isoelectric points were calculated for these sequences and plotted against one another using open source EMBOSS tools (Rice et al., 2000). For counting FGs, the lumenal and nucleoplasmic sequences were joined after removing transmembrane segments because NET FGs could also interact with many FG repeats on the transmembrane Nup gp210 that occurs in the NE lumen. NLS prediction scores were generated using PSORTII (Nakai and Horton, 1999).

Computational modeling of FRAP and PA experiments

Previous modeling of diffusion for a mobile cargo in an ER fragment used a particle-based simulation on a 3D reconstruction of the ER from multiple EM sections (Sbalzarini et al., 2005, 2006). Because we had to consider the entire cellular NE and ER, a similar level of detail could not be feasibly achieved. Thus, we simplified the model by representing the ER as a continuous sheet in 2D cross-section, with dimensions deduced from our HeLa cell images that were consistent with other measurements (Ribbeck and Görlich, 2001; Maeshima et al., 2010). This approximation is reasonably accurate for the interpretation of FRAP data, generally resulting in no more than a twofold underestimation of the diffusion coefficient for an integral ER protein (Sbalzarini et al., 2006). As this is on par with the typical levels of noise present in experimental data, we considered this approximation sufficient. Electron microscopy indicates many points of fusion between the ER and ONM, thus the kinetics of their protein exchange can be adequately represented by 2D diffusion. Considering spatial closeness of the ubiquitous NPCs (~425 nm apart) and the characteristic value of NET diffusion coefficients (~0.1 $\mu m^2/s$), we approximated the kinetics of ONM–INM exchange by a first-order reaction with kinetic rate k_1 independent of translocation direction. This assumption allowed us to reduce the double-membrane system to a single membrane in which freely diffusing proteins (not bound to immobile binding sites) are given by two distinct species with concentrations P^O and P^I, which stand for the ONM- and INM-localized proteins, respectively. Finally, to enable efficient numeric simulation, we represented cellular cross sections by a rectangular 2D domain as shown in Fig. S5. In this layout, two opposing boundaries with no-flux boundary conditions represent the double NE membrane and the plasma membrane, respectively, while the two other boundaries with periodic boundary conditions permit free diffusion around the nucleus. The y linear dimension of the domain was selected equal to the circumference of an average HeLa nucleus projection (~59 µm) while the x dimension was adjusted so that the area of the domain $S = x \times y$ was equal to the area of an average HeLa cell projection (minus the area of the nucleus projection) as estimated from our microscopy data (~841 μm^2). The slight spatial distortion introduced by this transformation can be neglected because the capacity of the ER (represented by the domain area) is preserved. To test the validity of this assumption, we also performed simulations using the public domain modeling platform Virtual Cell (Moraru et al., 2008), which allows simulation of diffusion on domains of arbitrary shape. Comparison of the FRAP and PA curves computed using the two different computational realizations of the model demonstrated virtually no differences, which supports the validity of our last assumption.

To model dynamics in the INM, we assumed the existence of a single type of immobile binding site (trap) with total concentration T_0. Thus, in addition to the P^O and P^I freely diffusing pools, there is the P^T-bound pool. The spatio-temporal dynamics of the system can then be described by four reaction–diffusion equations based on the mass-action rate law as follows:

$$\begin{aligned}
\partial P^O/\partial t &= k_1 P^I - k_1 P^O + D\,\partial^2 P^O/\partial r^2 \\
\partial P^I/\partial t &= k_1 P^O - k_1 P^I + k_{-2} P^T - k_2 P^I T + D\,\partial^2 P^I/\partial r^2 \\
\partial P^T/\partial t &= k_2 P^I T - k_{-2} P^T \\
\partial T/\partial t &= k_{-2} P^T - k_2 P^I T,
\end{aligned}$$

where T is the concentration of unoccupied binding sites, k_1 is the NPC translocation rate, k_2 and k_2 are the on- and off-rates of binding to the immobile binding sites, and D is the protein diffusion coefficient. Before bleaching or PA, the system is in the steady-state, therefore concentrations of the freely diffusing protein fractions are equilibrated across the ER, ONM, and INM; i.e., $P^{ER} = P^I = P^O$. At the same time:

$$\begin{aligned}
P^T &= k_2/k_{-2} P^I T \\
T + P^T &= T_0.
\end{aligned}$$

Published March 28, 2011

Solving these equations, we can find the ratio of the protein abundances in the ONM and INM as a function of the total concentration of the INM traps T_0 and the steady-state concentration of the free protein P^O:

$$\frac{P_{ONM}}{P_{INM}} = \frac{P^O}{P^I + P^T} = \alpha = \left(1 + \frac{K_2 T_0}{1 + K_2 P^O}\right)^{-1},$$

where $K_2 = k_2/k_{-2}$ is the trapping association constant. If trapping is strong ($K_2 \gg 1$), all binding sites in the INM are saturated and the ratio α becomes simply:

$$\alpha = \frac{P^O}{P^O + T_0}.$$

To constrain the model, where possible, we used values of α derived from the immuno-gold EM data presented in this study or published results (Senior and Gerace, 1988). Assuming that the value of α is given, the total concentration of traps, T_0, can then be expressed from the last two equations as a function of the parameter K_2 and the steady-state concentration P^0 as simply:

$$T_0 = \frac{1-\alpha}{\alpha} \cdot \frac{1 + K_2 P^O}{K_2}.$$

Note that because both FRAP and PA data are expressed in nondimensional relative units, the unknown absolute value P^0 is irrelevant and can be chosen to be any arbitrary value suitable for numeric simulations (e.g., 10 µM in our simulations). Therefore, with the value of α fixed, the total number of free model parameters to be found from fitting to the experimental data are reduced to only four, namely, the diffusion coefficient D and the three reaction rates k_1, k_2, and k_{-2}.

To model FRAP and PA, we introduced variables representing bleached/activated counterparts of P^O, P^I, and P^T. Initial conditions were chosen to match the spatial masks in the FRAP/PA experiments, and the spatio-temporal evolution of the system was calculated numerically using a standard finite difference method implemented as a custom C code. Computed FRAP and PA curves were then fitted to the experimental data using the standard least mean squares procedure. We found that even after gross simplifications of the model introduced in this study, the available data did not fully constrain all the parameters. Thus, in the case of strong trapping, the on-rate of binding is essentially irrelevant as far as $K_2 \gg 1$ and, therefore, cannot be inferred from the available data. This parameter, however, is not significant, as it does not affect the observed system dynamics. Instead, we chose to concentrate on the parameters k_1 and k_{-2}, which are inversely proportional to the characteristic half-life times of the NPC translocation and trapping by binding in the INM, respectively. As these parameters determine the long-term kinetics of FRAP and PA, we were able to estimate them with the accuracy commensurate with that of our experimental measurements.

Online supplemental material

Fig. S1 shows NE and ER FRAP for all NETs Fig. S2 shows the relationship between $t_{1/2}$s and mobile fractions. Fig. S3 shows PA of LAP1-L. Fig. S4 shows that RanQ69L likely affects the translocation step of LBR Fig. S5 shows construction of the spatial domain for the computational model. Table S1 shows statistical results from the χ^2 test for Fig. 5 EM data. Table S2 shows the statistical results from the Kolmogorov-Smirnov test against the hypothesis that any two datasets are different for Fig. 7 data. Online supplemental material is available at http://www.jcb.org/cgi/content/full/jcb.201009068/DC1.

We would like to thank Elena Buss for cloning assistance, Didier Hodzic and Tom Rapoport for expression plasmids, Stephen Mitchell and Helen Grindley for technical assistance, and Lars Schmiedeberg for advice and critical reading of the manuscript.

The authors declare no conflicts of interest. This study was supported by a Wellcome Trust Senior Research Fellowship to E.C. Schirmer, the University of Edinburgh Staff Scholarship Scheme to N. Zuleger, and Biotechnology and Biological Sciences Research Council UK grant BB/E015735/1 to M.W. Goldberg.

Submitted: 13 September 2010
Accepted: 8 March 2011

References

Alber, F., S. Dokudovskaya, L.M. Veenhoff, W. Zhang, J. Kipper, D. Devos, A. Suprapto, O. Karni-Schmidt, R. Williams, B.T. Chait, et al. 2007. The molecular architecture of the nuclear pore complex. *Nature*. 450:695–701. doi:10.1038/nature06405

Braunagel, S.C., S.T. Williamson, Q. Ding, X. Wu, and M.D. Summers. 2007. Early sorting of inner nuclear membrane proteins is conserved. *Proc. Natl. Acad. Sci. USA*. 104:9307–9312. doi:10.1073/pnas.0703186104

Callan, H.G., J.T. Randall, and S.G. Tomlin. 1949. An electron microscope study of the nuclear membrane. *Nature*. 163:280. doi:10.1038/163280a0

Campbell, R.E., O. Tour, A.E. Palmer, P.A. Steinbach, G.S. Baird, D.A. Zacharias, and R.Y. Tsien. 2002. A monomeric red fluorescent protein. *Proc. Natl. Acad. Sci. USA*. 99:7877–7882. doi:10.1073/pnas.082243699

Cartegni, L., M.R. di Barletta, R. Barresi, S. Squarzoni, P. Sabatelli, N. Maraldi, M. Mora, C. Di Blasi, F. Cornelio, L. Merlini, et al. 1997. Heart-specific localization of emerin: new insights into Emery-Dreifuss muscular dystrophy. *Hum. Mol. Genet.* 6:2257–2264. doi:10.1093/hmg/6.13.2257

Clements, L., S. Manilal, D.R. Love, and G.E. Morris. 2000. Direct interaction between emerin and lamin A. *Biochem. Biophys. Res. Commun.* 267:709–714. doi:10.1006/bbrc.1999.2023

Deng, M., and M. Hochstrasser. 2006. Spatially regulated ubiquitin ligation by an ER/nuclear membrane ligase. *Nature*. 443:827–831. doi:10.1038/nature05170

Dickmanns, A., F.R. Bischoff, C. Marshallsay, R. Lührmann, H. Ponstingl, and E. Fanning. 1996. The thermolability of nuclear protein import in tsBN2 cells is suppressed by microinjected Ran-GTP or Ran-GDP, but not by RanQ69L or RanT24N. *J. Cell Sci.* 109:1449–1457.

Ellenberg, J., E.D. Siggia, J.E. Moreira, C.L. Smith, J.F. Presley, H.J. Worman, and J. Lippincott-Schwartz. 1997. Nuclear membrane dynamics and reassembly in living cells: targeting of an inner nuclear membrane protein in interphase and mitosis. *J. Cell Biol.* 138:1193–1206. doi:10.1083/jcb.138.6.1193

Foisner, R., and L. Gerace. 1993. Integral membrane proteins of the nuclear envelope interact with lamins and chromosomes, and binding is modulated by mitotic phosphorylation. *Cell*. 73:1267–1279. doi:10.1016/0092-8674(93)90355-T

Goldfarb, D.S., J. Gariépy, G. Schoolnik, and R.D. Kornberg. 1986. Synthetic peptides as nuclear localization signals. *Nature*. 322:641–644. doi:10.1038/322641a0

Goodchild, R.E., and W.T. Dauer. 2005. The AAA+ protein torsinA interacts with a conserved domain present in LAP1 and a novel ER protein. *J. Cell Biol.* 168:855–862. doi:10.1083/jcb.200411026

Gruenbaum, Y., A. Margalit, R.D. Goldman, D.K. Shumaker, and K.L. Wilson. 2005. The nuclear lamina comes of age. *Nat. Rev. Mol. Cell Biol.* 6:21–31. doi:10.1038/nrm1550

Hawryluk-Gara, L.A., E.K. Shibuya, and R.W. Wozniak. 2005. Vertebrate Nup53 interacts with the nuclear lamina and is required for the assembly of a Nup93-containing complex. *Mol. Biol. Cell*. 16:2382–2394. doi:10.1091/mbc.E04-10-0857

Hinshaw, J.E., B.O. Carragher, and R.A. Milligan. 1992. Architecture and design of the nuclear pore complex. *Cell*. 69:1133–1141. doi:10.1016/0092-8674(92)90635-P

Hodzic, D.M., D.B. Yeater, L. Bengtsson, H. Otto, and P.D. Stahl. 2004. Sun2 is a novel mammalian inner nuclear membrane protein. *J. Biol. Chem.* 279:25805–25812. doi:10.1074/jbc.M313157200

King, M.C., C.P. Lusk, and G. Blobel. 2006. Karyopherin-mediated import of integral inner nuclear membrane proteins. *Nature*. 442:1003–1007. doi:10.1038/nature05075

Krogh, A., B. Larsson, G. von Heijne, and E.L. Sonnhammer. 2001. Predicting transmembrane protein topology with a hidden Markov model: application to complete genomes. *J. Mol. Biol.* 305:567–580. doi:10.1006/jmbi.2000.4315

Lattanzi, G., A. Ognibene, P. Sabatelli, C. Capanni, D. Toniolo, M. Columbaro, S. Santi, M. Riccio, L. Merlini, N.M. Maraldi, and S. Squarzoni. 2000. Emerin expression at the early stages of myogenic differentiation. *Differentiation*. 66:208–217. doi:10.1111/j.1432-0436.2000.660407.x

Ma, Y., S. Cai, Q. Lv, Q. Jiang, Q. Zhang, Z. Sodmergen, Z. Zhai, and C. Zhang. 2007. Lamin B receptor plays a role in stimulating nuclear envelope production and targeting membrane vesicles to chromatin during nuclear envelope assembly through direct interaction with importin beta. *J. Cell Sci.* 120:520–530. doi:10.1242/jcs.03355

Maeshima, K., H. Iino, S. Hihara, T. Funakoshi, A. Watanabe, M. Nishimura, R. Nakatomi, K. Yahata, F. Imamoto, T. Hashikawa, et al. 2010. Nuclear pore formation but not nuclear growth is governed by cyclin-dependent kinases (Cdks) during interphase. *Nat. Struct. Mol. Biol.* 17:1065–1071. doi:10.1038/nsmb.1878

Malik, P., N. Korfali, V. Srsen, V. Lazou, D.G. Batrakou, N. Zuleger, D.M. Kavanagh, G.S. Wilkie, M.W. Goldberg, and E.C. Schirmer. 2010. Cell-specific and lamin-dependent targeting of novel transmembrane proteins in the nuclear envelope. *Cell. Mol. Life Sci.* 67:1353–1369. doi:10.1007/s00018-010-0257-2

Marelli, M., J.D. Aitchison, and R.W. Wozniak. 1998. Specific binding of the karyopherin Kap121p to a subunit of the nuclear pore complex containing Nup53p, Nup59p, and Nup170p. *J. Cell Biol.* 143:1813–1830. doi:10.1083/jcb.143.7.1813

Martin, L., C. Crimaudo, and L. Gerace. 1995. cDNA cloning and characterization of lamina-associated polypeptide 1C (LAP1C), an integral protein of the inner nuclear membrane. *J. Biol. Chem.* 270:8822–8828. doi:10.1074/jbc.270.15.8822

Mattout-Drubezki, A., and Y. Gruenbaum. 2003. Dynamic interactions of nuclear lamina proteins with chromatin and transcriptional machinery. *Cell. Mol. Life Sci.* 60:2053–2063. doi:10.1007/s00018-003-3038-3

Mootha, V.K., J. Bunkenborg, J.V. Olsen, M. Hjerrild, J.R. Wisniewski, E. Stahl, M.S. Bolouri, H.N. Ray, S. Sihag, M. Kamal, et al. 2003. Integrated analysis of protein composition, tissue diversity, and gene regulation in mouse mitochondria. *Cell*. 115:629–640. doi:10.1016/S0092-8674(03)00926-7

Moraru, I.I., J.C. Schaff, B.M. Slepchenko, M.L. Blinov, F. Morgan, A. Lakshminarayana, F. Gao, Y. Li, and L.M. Loew. 2008. Virtual Cell modelling and simulation software environment. *IET Syst. Biol.* 2:352–362. doi:10.1049/iet-syb:20080102

Nakai, K., and P. Horton. 1999. PSORT: a program for detecting sorting signals in proteins and predicting their subcellular localization. *Trends Biochem. Sci.* 24:34–36. doi:10.1016/S0968-0004(98)01336-X

Ohba, T., E.C. Schirmer, T. Nishimoto, and L. Gerace. 2004. Energy- and temperature-dependent transport of integral proteins to the inner nuclear membrane via the nuclear pore. *J. Cell Biol.* 167:1051–1062. doi:10.1083/jcb.200409149

Ostlund, C., J. Ellenberg, E. Hallberg, J. Lippincott-Schwartz, and H.J. Worman. 1999. Intracellular trafficking of emerin, the Emery-Dreifuss muscular dystrophy protein. *J. Cell Sci.* 112:1709–1719.

Patterson, G.H., and J. Lippincott-Schwartz. 2002. A photoactivatable GFP for selective photolabeling of proteins and cells. *Science*. 297:1873–1877. doi:10.1126/science.1074952

Phair, R.D., and T. Misteli. 2001. Kinetic modelling approaches to in vivo imaging. *Nat. Rev. Mol. Cell Biol.* 2:898–907. doi:10.1038/35103000

Powell, L., and B. Burke. 1990. Internuclear exchange of an inner nuclear membrane protein (p55) in heterokaryons: in vivo evidence for the interaction of p55 with the nuclear lamina. *J. Cell Biol.* 111:2225–2234. doi:10.1083/jcb.111.6.2225

Prunuske, A.J., and K.S. Ullman. 2006. The nuclear envelope: form and reformation. *Curr. Opin. Cell Biol.* 18:108–116. doi:10.1016/j.ceb.2005.12.004

Reichelt, R., A. Holzenburg, E.L. Buhle Jr., M. Jarnik, A. Engel, and U. Aebi. 1990. Correlation between structure and mass distribution of the nuclear pore complex and of distinct pore complex components. *J. Cell Biol.* 110:883–894. doi:10.1083/jcb.110.4.883

Rexach, M., and G. Blobel. 1995. Protein import into nuclei: association and dissociation reactions involving transport substrate, transport factors, and nucleoporins. *Cell*. 83:683–692. doi:10.1016/0092-8674(95)90181-7

Ribbeck, K., and D. Görlich. 2001. Kinetic analysis of translocation through nuclear pore complexes. *EMBO J.* 20:1320–1330. doi:10.1093/emboj/20.6.1320

Rice, P., I. Longden, and A. Bleasby. 2000. EMBOSS: the European Molecular Biology Open Software Suite. *Trends Genet.* 16:276–277. doi:10.1016/S0168-9525(00)02024-2

Rolls, M.M., P.A. Stein, S.S. Taylor, E. Ha, F. McKeon, and T.A. Rapoport. 1999. A visual screen of a GFP-fusion library identifies a new type of nuclear envelope membrane protein. *J. Cell Biol.* 146:29–44.

Sakaki, M., H. Koike, N. Takahashi, N. Sasagawa, S. Tomioka, K. Arahata, and S. Ishiura. 2001. Interaction between emerin and nuclear lamins. *J. Biochem.* 129:321–327.

Saksena, S., Y. Shao, S.C. Braunagel, M.D. Summers, and A.E. Johnson. 2004. Cotranslational integration and initial sorting at the endoplasmic reticulum translocon of proteins destined for the inner nuclear membrane. *Proc. Natl. Acad. Sci. USA*. 101:12537–12542. doi:10.1073/pnas.0404934101

Saksena, S., M.D. Summers, J.K. Burks, A.E. Johnson, and S.C. Braunagel. 2006. Importin-alpha-16 is a translocon-associated protein involved in sorting membrane proteins to the nuclear envelope. *Nat. Struct. Mol. Biol.* 13:500–508. doi:10.1038/nsmb1098

Salpingidou, G., A. Smertenko, I. Hausmanowa-Petrucewicz, P.J. Hussey, and C.J. Hutchison. 2007. A novel role for the nuclear membrane protein emerin in association of the centrosome to the outer nuclear membrane. *J. Cell Biol.* 178:897–904. doi:10.1083/jcb.200702026

Sbalzarini, I.F., A. Mezzacasa, A. Helenius, and P. Koumoutsakos. 2005. Effects of organelle shape on fluorescence recovery after photobleaching. *Biophys. J.* 89:1482–1492. doi:10.1529/biophysj.104.057885

Sbalzarini, I.F., A. Hayer, A. Helenius, and P. Koumoutsakos. 2006. Simulations of (an)isotropic diffusion on curved biological surfaces. *Biophys. J.* 90:878–885. doi:10.1529/biophysj.105.073809

Schirmer, E.C., and R. Foisner. 2007. Proteins that associate with lamins: many faces, many functions. *Exp. Cell Res.* 313:2167–2179. doi:10.1016/j.yexcr.2007.03.012

Schirmer, E.C., L. Florens, T. Guan, J.R. Yates III, and L. Gerace. 2003. Nuclear membrane proteins with potential disease links found by subtractive proteomics. *Science*. 301:1380–1382. doi:10.1126/science.1088176

Senior, A., and L. Gerace. 1988. Integral membrane proteins specific to the inner nuclear membrane and associated with the nuclear lamina. *J. Cell Biol.* 107:2029–2036. doi:10.1083/jcb.107.6.2029

Shimi, T., T. Koujin, M. Segura-Totten, K.L. Wilson, T. Haraguchi, and Y. Hiraoka. 2004. Dynamic interaction between BAF and emerin revealed by FRAP, FLIP, and FRET analyses in living HeLa cells. *J. Struct. Biol.* 147:31–41. doi:10.1016/j.jsb.2003.11.013

Silljé, H.H., S. Nagel, R. Körner, and E.A. Nigg. 2006. HURP is a Ran-importin beta-regulated protein that stabilizes kinetochore microtubules in the vicinity of chromosomes. *Curr. Biol.* 16:731–742. doi:10.1016/j.cub.2006.02.070

Smith, S., and G. Blobel. 1994. Colocalization of vertebrate lamin B and lamin B receptor (LBR) in nuclear envelopes and in LBR-induced membrane stacks of the yeast *Saccharomyces cerevisiae. Proc. Natl. Acad. Sci. USA*. 91:10124–10128. doi:10.1073/pnas.91.21.10124

Soullam, B., and H.J. Worman. 1993. The amino-terminal domain of the lamin B receptor is a nuclear envelope targeting signal. *J. Cell Biol.* 120:1093–1100. doi:10.1083/jcb.120.5.1093

Soullam, B., and H.J. Worman. 1995. Signals and structural features involved in integral membrane protein targeting to the inner nuclear membrane. *J. Cell Biol.* 130:15–27. doi:10.1083/jcb.130.1.15

Squarzoni, S., P. Sabatelli, A. Ognibene, D. Toniolo, L. Cartegni, F. Cobianchi, S. Petrini, L. Merlini, and N.M. Maraldi. 1998. Immunocytochemical detection of emerin within the nuclear matrix. *Neuromuscul. Disord.* 8:338–344. doi:10.1016/S0960-8966(98)00031-5

Suntharalingam, M., and S.R. Wente. 2003. Peering through the pore: nuclear pore complex structure, assembly, and function. *Dev. Cell*. 4:775–789. doi:10.1016/S1534-5807(03)00162-X

Theerthagiri, G., N. Eisenhardt, H. Schwarz, and W. Antonin. 2010. The nucleoporin Nup188 controls passage of membrane proteins across the nuclear pore complex. *J. Cell Biol.* 189:1129–1142. doi:10.1083/jcb.200912045

Turgay, Y., R. Ungricht, A. Rothballer, A. Kiss, G. Csucs, P. Horvath, and U. Kutay. 2010. A classical NLS and the SUN domain contribute to the targeting of SUN2 to the inner nuclear membrane. *EMBO J.* 29:2262–2275. doi:10.1038/emboj.2010.119

Ulbert, S., M. Platani, S. Boue, and I.W. Mattaj. 2006. Direct membrane protein-DNA interactions required early in nuclear envelope assembly. *J. Cell Biol.* 173:469–476. doi:10.1083/jcb.200512078

Worman, H.J., J. Yuan, G. Blobel, and S.D. Georgatos. 1988. A lamin B receptor in the nuclear envelope. *Proc. Natl. Acad. Sci. USA*. 85:8531–8534. doi:10.1073/pnas.85.22.8531

Wu, W., F. Lin, and H.J. Worman. 2002. Intracellular trafficking of MAN1, an integral protein of the nuclear envelope inner membrane. *J. Cell Sci.* 115:1361–1371.

Wychowski, C., D. Benichou, and M. Girard. 1986. A domain of SV40 capsid polypeptide VP1 that specifies migration into the cell nucleus. *EMBO J.* 5:2569–2576.

Ye, Q., and H.J. Worman. 1996. Interaction between an integral protein of the nuclear envelope inner membrane and human chromodomain proteins homologous to *Drosophila* HP1. *J. Biol. Chem.* 271:14653–14656. doi:10.1074/jbc.271.25.14653